

Effect of Mirror Quality on Optical Response of Nanoparticle-on-Mirror Plasmonic Nanocavities

Zhenxin Wang, Lufang Liu, Di Zhang, Alexey V. Krasavin, Junsheng Zheng, Chenxinyu Pan, Enxing He, Zifan Wang, Shengchengao Zhong, Zhiyong Li, Mengxin Ren, Xin Guo, Anatoly V. Zayats, Limin Tong, and Pan Wang*

As an essential part of nanoparticle-on-mirror (NPoM) plasmonic nanocavities, metal mirrors play an important role not only in determining the optical response of the nanocavities but also their application performance. Here the effect of mirror quality on the optical response of nanosphere-on-mirror (NSoM) and nanocube-on-mirror (NCoM) nanocavities is experimentally studied. Polycrystalline sputtered gold films (SGFs), template-stripped gold films (TSGFs), and single-crystalline gold microflakes (GMFs) are investigated and compared. Due to the great improvement in the surface roughness that can minimize fluctuations in the gap morphology, NSoM and NCoM nanocavities formed on smooth TSGFs and GMFs have a better cavity-to-cavity homogeneity in the scattering spectrum than those formed on comparably rougher SGFs. In addition, there is an obvious change in the spectral positions of the resonance modes of NSoM and NCoM nanocavities formed on SGFs due to the variation in the gap morphology, which is reproduced very well by theoretical calculations based on measured dielectric functions of the gold films. Finally, due to the reduction in electron scattering losses from SGFs to TSGFs and GMFs, an increase in the quality factors and scattering intensities of the resonance modes is observed for nanocavities formed on the corresponding films.

enhancement.^[1–3] They have been used for a variety of applications ranging from biochemical sensing and plasmon-enhanced spectroscopies to nonlinear optics and nanolasers.^[4–13] Particularly, among the plethora of developed plasmonic nanostructures, nanoparticle-on-mirror (NPoM) plasmonic nanocavities, consisting of a metal nanoparticle placed on a metal mirror and separated by a dielectric spacer,^[2,14,15] have recently attracted significant research interest because of their ability to provide extreme optical confinement combined with the ease of fabrication. Therefore, they offer an attractive platform for the study of light-matter interactions at the nanoscale and have triggered a series of breakthroughs in state-of-the-art nanophotonic research and applications, including enhancement of spontaneous emission^[16–19] and nonlinearities,^[20] high-sensitivity optical sensing,^[21,22] strong coupling,^[23,24] and quantum plasmonics.^[3,25–27] In the theoretical description of the optical response of


1. Introduction

Metallic nanostructures, which support localized surface plasmons (LSPs) by coupling optical fields with collective oscillations of free electrons, can squeeze light into deep-subwavelength volumes and provide considerable local-field

NPoM nanocavities, as their key component, the metal mirror is usually treated as an ideal metal film with an ultimately smooth surface. In this case, the optical response is mainly determined by the size and shape of the nanoparticles, thickness of the spacers, as well as their dielectric properties.^[28–31] However, in practice, NPoM nanocavities are fabricated

Z. Wang, L. Liu, J. Zheng, C. Pan, E. He, Z. Wang, S. Zhong, Z. Li, X. Guo, L. Tong, P. Wang
 State Key Laboratory of Modern Optical Instrumentation
 College of Optical Science and Engineering
 Zhejiang University
 Hangzhou 310027, China
 E-mail: nanopan@zju.edu.cn

D. Zhang, M. Ren
 The Key Laboratory of Weak-Light Nonlinear Photonics
 Ministry of Education
 School of Physics and TEDA Applied Physics Institute
 Nankai University
 Tianjin 300071, China

 The ORCID identification number(s) for the author(s) of this article can be found under <https://doi.org/10.1002/adom.202201914>.

DOI: 10.1002/adom.202201914

A. V. Krasavin, A. V. Zayats
 Department of Physics and London Centre for Nanotechnology
 King's College London
 London WC2R 2LS, UK

Z. Li, X. Guo, P. Wang
 Jiaxing Key Laboratory of Photonic Sensing & Intelligent Imaging
 Jiaxing Institute Zhejiang University
 Jiaxing 314000, China

Z. Li, X. Guo, P. Wang
 Intelligent Optics & Photonics Research Center
 Jiaxing Institute Zhejiang University
 Jiaxing 314000, China

L. Tong
 Collaborative Innovation Center of Extreme Optics
 Shanxi University
 Taiyuan 030006, China

using deposited polycrystalline metal films with a rough surface^[16,18,23,24,26,32–35] or template-stripped polycrystalline metal films with a very smooth surface as the mirrors.^[17,36,37] Recently, chemically grown single-crystalline gold microflakes (GMFs) with an ultrasmooth surface have been exploited as the metal mirrors as well, providing NPoM nanocavities with significantly reduced loss.^[38,39]

Due to the strong confinement of optical fields in the nanometer-scale gap, the optical response of NPoM nanocavities is extremely sensitive to the nanoscale morphology of the metallic gap as well as the crystalline quality of the metal mirror. A small change in the gap morphology induced by a rough mirror surface may introduce a significant fluctuation in the spectral position of the plasmonic resonances, while the scattering of electrons by surface roughness and numerous grain boundaries can cause a significant optical loss and resonance broadening.^[39,40] Therefore, it is necessary to investigate the effect of the mirror quality on the optical response of NPoM nanocavities, which will benefit both the fundamental understanding of nanocavity properties, and the optimized design of nanocavity-based plasmonic devices to achieve better performances in practical applications.

In this work, we systematically investigate the effect of mirror quality on the optical response of NPoM nanocavities including nanosphere-on-mirror (NSoM) nanocavities with a point-contact gap and nanocube-on-mirror (NCoM) nanocavities with a face-contact gap. Three typical types of gold films are implemented as the mirrors, which are polycrystalline sputtered gold films (SGFs) with a rough surface together with polycrystalline template-stripped gold films (TSGFs) and single-crystalline GMFs with ultrasmooth surfaces. Compared with NSoM and NCoM nanocavities formed on SGFs, nanocavities formed on TSGFs and GMFs have a better cavity-to-cavity homogeneity in the scattering spectrum, which is due to the great improvement in the surface roughness of TSGFs and GMFs that can minimize the fluctuation in the gap morphology. In addition, there is an obvious change in the peak wavelengths of the resonance modes of the NSoM and NCoM nanocavities formed on different gold films due to the variation in dielectric functions and surface qualities of the gold films. These are reproduced very well by theoretical calculations based on experimentally measured dielectric functions of the SGFs, TSGFs, and GMFs. Moreover, due to the reduction in electron scattering losses (introduced by surface roughness and grain boundaries) from SGFs to TSGFs and GMFs, there is an increase in the quality factors and scattering intensities of the resonant modes for both NSoM and NCoM nanocavities.

2. Preparation and Characterization of Different Gold Mirrors

For a fair comparison, in the experiments the thicknesses of the gold films were kept the same as 50 nm. Details of the fabrication of the gold films can be found in Experimental Section. Figure 1d–f presents the surface morphologies of an SGF, a TSGF, and a GMF (scanning electron microscopy (SEM) images are shown in Figure S1 in the Supporting Information). It can be clearly seen that the surface of the SGF shows an uneven

landscape with a measured root-mean-square (RMS) roughness of ≈ 1.6 nm (Figure 1d), which is due to the island growth of gold during the sputtering process. In contrast, the surface of the TSGF (Figure 1e), determined by the surface quality of the substrate used for deposition (silicon wafer with 300 nm oxide layer in our case), is much smoother and has an RMS roughness of ≈ 0.14 nm. The stark contrast in the surface quality for the upper and bottom surfaces of a gold film sputtered on the silicon substrate can be further visualized with the transmission electron microscopy (TEM) images (Figure 1g,h) of the cross section of the film, which displays nanometer-scale fluctuations for the upper surface. The nonperiodic lattice fringes observed in the high-resolution TEM image of the sputtered gold film (Figure 1i) indicate that both SGFs and TSGFs have a polycrystalline structure. Different from SGFs and TSGFs, in agreement with previous works,^[39,41] chemically grown GMFs have a single-crystalline structure and an atomically smooth surface with an RMS roughness as low as ≈ 0.16 nm (Figure 1f).

In addition to the structural characteristics, we further compared the dielectric functions of the studied gold films (see Experimental Section for details). Their thicknesses were chosen to be ≈ 200 nm, so their optical properties are essentially that of a bulk material. Figure 1j shows the real (ϵ_1) and imaginary (ϵ_2) parts of the dielectric functions for the SGFs (green line), TSGFs (blue line) and GMFs (red line) measured in the wavelength range from 400 to 980 nm. For comparison, data from Johnson and Christy^[42] and Olmon et al.^[43] are plotted as well in Figure S2 (Supporting Information). As shown in Figure 1j, there is an increase in the value of $|\epsilon_1|$ from SGF to TSGF and GMF, which is due to the increase in their conductivities. For the value of ϵ_2 , in the short-wavelength region below 516 nm, it is dominated by the electronic interband transitions from the occupied d bands to the partially filled sp bands in gold. Therefore, the value of ϵ_2 increases from SGF to TSGF and GMF in this wavelength range due to the decrease in the effective volume density of voids for the gold films.^[44] In the long-wavelength region above 700 nm, the GMF with a single-crystalline structure and an atomically smooth surface has the smallest value of ϵ_2 due to the greatly reduced scattering of electrons introduced by surface roughness and grain boundaries. However, the value of ϵ_2 for the TSGF with a smooth surface is larger than that of the SGF in this wavelength region. This agrees well with the data from Olmon et al.,^[43] and in our view this can be related to the variation of the grain size during the deposition process, so the grain sizes at the measured interface are different for the TSGF and SGF.

3. NSoM Nanocavities with a Point-Contact Gap

3.1. Experimental Results

We first investigated the effect of mirror quality on the optical response of point-contact-type (a single contact point) NPoM nanocavities such as NSoM nanocavities. Experimentally, gold nanospheres (synthesized by a successive seed-mediated growth method^[45]), with a truly spherical shape and an average

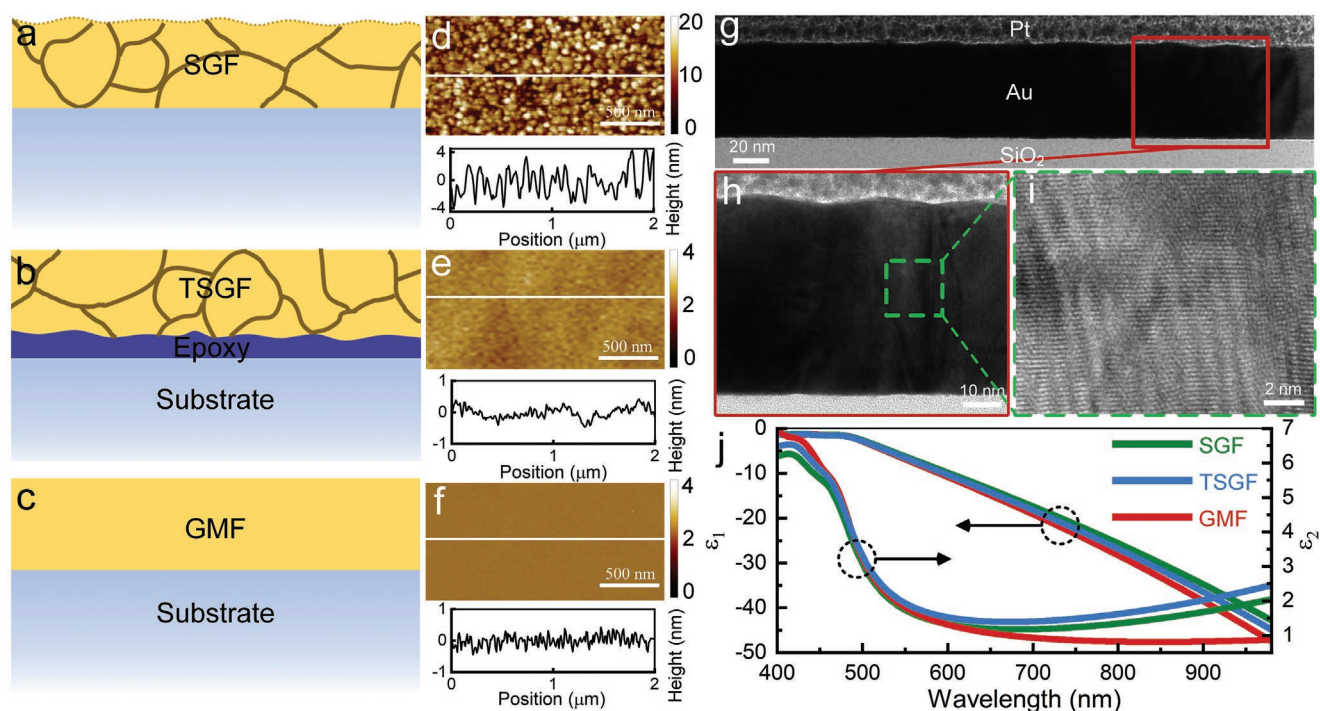


Figure 1. Characteristics of three representative types of gold mirrors. a–c) Schematic illustrations of a) an SGF, b) a TSGF, and c) a GMF. Brown lines in panels (a) and (b) represent grain boundaries. d–f) AFM images and line scans along the indicated white lines for d) an SGF, e) a TSGF, and f) a GMF with the same thickness of 50 nm. g) Cross-sectional TEM image of an SGF (50 nm in thickness) after focused ion beam milling. h) Close-up view of the region marked with a red rectangle in panel (g). i) Atomically resolved TEM image of the region marked with a green dashed square in (h). j) Measured dielectric functions (left: real part ϵ_1 ; right: imaginary part ϵ_2) of an SGF, a TSGF, and a GMF with the same thickness of ≈ 200 nm.

diameter of 69 ± 4 nm (Figure S3, Supporting Information), were used to construct the NSoM nanocavities to minimize the effect of the nanoparticle size and shape distributions. Each nanosphere is capped with a bilayer of cetyltrimethylammonium chloride (CTAC) having a thickness of ≈ 1 nm (Figure S3c, Supporting Information). By drop-casting a diluted solution of the gold nanospheres onto the gold films, well-separated individual NSoM nanocavities with a total gap thickness of ≈ 1 nm can be obtained (note that the gap morphology is affected by the surface roughness for nanocavities formed on SGFs). **Figure 2a–c** shows typical dark-field scattering images (see Section S4 in the Supporting Information for details) of the NSoM nanocavities formed on an SGF, a TSGF, and a GMF with the same thickness of ≈ 50 nm. Each nanocavity exhibits a scattering image consisting of both green (in the middle) and red (with a doughnut-shaped spatial distribution) scattering components. It can clearly be seen that the scattering images of the nanocavities formed on the TSGF and GMF are more uniform than those formed on the SGF, and that the nanocavities formed on the GMF have the highest scattering intensity.

To quantitatively investigate the effect of mirror quality on the optical response of the NSoM nanocavities, dark-field scattering spectra of ≈ 100 nanocavities of each type were measured. The scattering spectra of the NSoM nanocavities (Figure 2d–f; Figure S5, Supporting Information) display a dominating peak at around 700 nm (labeled as mode V), which corresponds to the excitation of film-coupled vertical dipolar mode of the

nanosphere.^[28,46] In addition, there is a relatively weak peak located around 550 nm (labeled as mode M), which corresponds to the excitation of a film-coupled quadrupolar mode of the nanosphere. Note that a new peak at around 640 nm (circled by dashed orange lines in the superimposed scattering spectra in Figure S5 of the Supporting Information) emerges for some of the nanocavities constructed on GMFs and TSGFs (relatively weak in this case), which is due to the existence of a small number of aspheric nanoparticles with an ellipsoidal shape in the synthesized gold nanospheres (see Figure S3a in the Supporting Information). These nanoparticles can form an elongated contact area with the mirror, which can therefore produce the new distinctive resonance mode at around 640 nm corresponding to the excitation of film-coupled longitudinal mode of the nanoparticle.^[47] The absence of this peak in the scattering spectra of nanocavities constructed on SGFs is mainly due to the larger electron scattering losses from the rough surface and grain boundaries of the SGFs. Similarly, despite the TSGFs and GMFs have the same-level surface quality, this peak is weaker in NSoM nanocavities formed on TSGFs (compare Figure S5b and Figure S5c in the Supporting Information) due to the existence of grain-boundary-induced electron scattering loss. It is obvious that the cavity-to-cavity homogeneity in the scattering spectra of nanocavities formed on TSGFs and GMFs is much better than that of nanocavities formed on SGFs (Figure 2d–f; Figure S5, Supporting Information). Also, the dominating resonance mode, i.e., mode V, of the nanocavities formed on the GMFs exhibits a narrower linewidth.

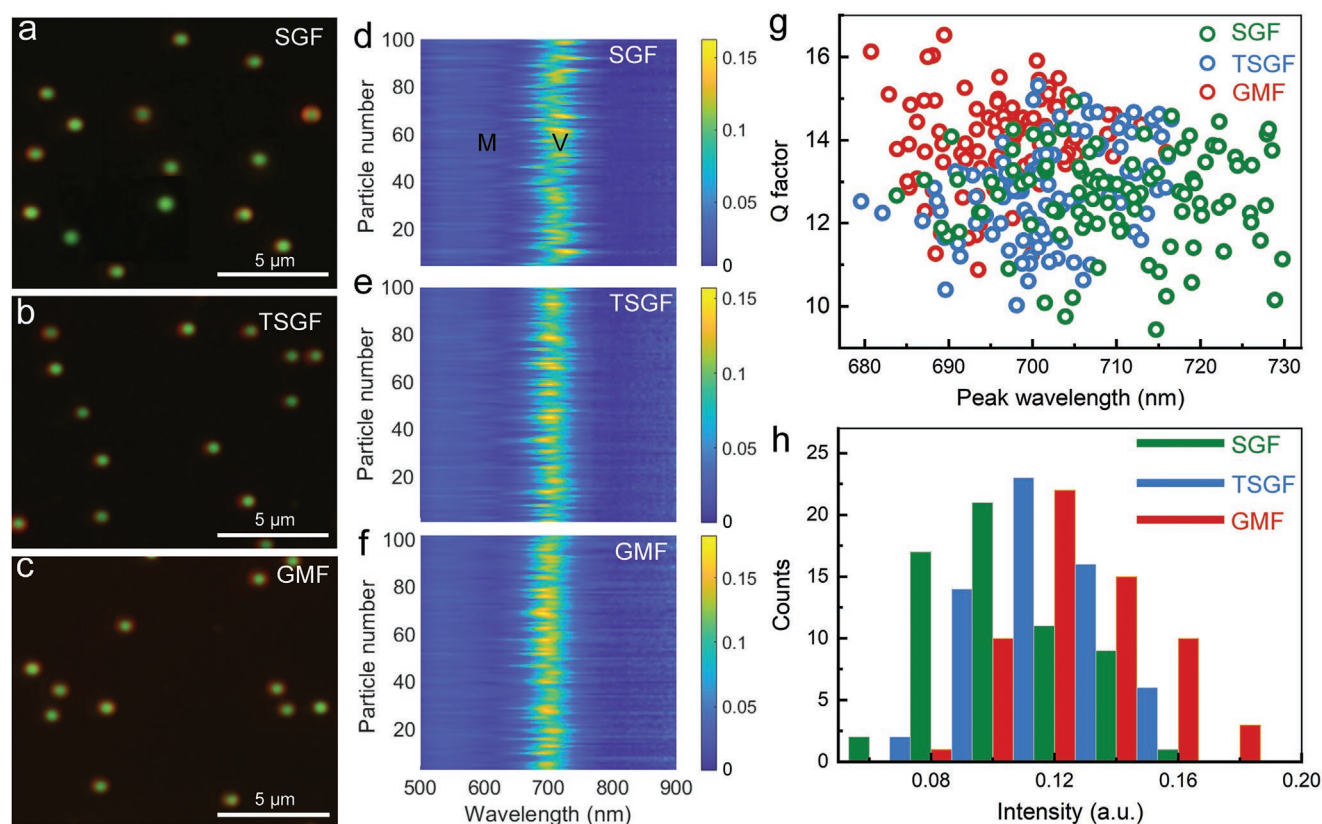


Figure 2. Statistical analysis of the effect of mirror quality on the optical response of the NSoM nanocavities. a–c) Dark-field scattering images of the NSoM nanocavities formed on a) an SGF, b) a TSGF, and c) a GMF with the same thicknesses of ≈ 50 nm. d–f) Waterfall plot of dark-field scattering spectra of the 100 nanocavities formed on the d) SGFs, e) TSGFs, f) GMFs. g) Statistical plot of the resonant wavelength and quality factors of mode V (extracted from the scattering spectra shown in panels (d)–(f)) for nanocavities formed on the SGFs (green), TSGFs (blue), and GMFs (red). h) Histogram of peak scattering intensities (extracted from the scattering spectra shown in panels (d)–(f)) of mode V for the nanocavities formed on the SGFs (green), TSGFs (blue), and GMFs (red).

This can be seen more intuitively in a statistic plot of the peak wavelengths and quality factors of the resonance mode V (see Section S7 in the Supporting Information for calculation details) for each type of the nanocavity (Figure 2g; Table S1, Supporting Information). The average peak wavelengths of mode V for nanocavities formed on the SGFs, TSGFs, and GMFs are found to be 712.2 ± 11.9 , 702.9 ± 7.9 , and 699.2 ± 7.2 nm, respectively. Nanocavities formed on TSGFs and GMFs have a better homogeneity in the scattering spectrum due to the great improvement in their surface quality compared with SGFs, which minimizes the fluctuation in the gap morphology (e.g., its shape and average thickness), affecting the optical response of the nanocavities. In addition, compared with the nanocavities formed on the TSGFs and GMFs, there is an obvious redshift (≈ 13 nm) in the average peak wavelength for the nanocavities formed on the SGFs. This is caused by the difference in the gap morphology for the NSoM nanocavities formed on the rough (i.e., SGFs) and smooth (i.e., TSGFs and GMFs) gold mirrors, which will be discussed in detail in the following sections. The average quality factors of mode V for nanocavities formed on the SGFs, TSGFs, and GMFs are calculated to be 12.52 ± 1.38 , 13.06 ± 1.17 , and 13.95 ± 1.19 , respectively. The gradual improvement in the quality factors for the three types of the gold mirrors can be attributed to the reduction in electron scattering

losses introduced by grain boundaries and surface roughness, which are significant in SGFs and TSGFs. The analysis of the statistics also quantifies an ≈ 1.2 times increase in the scattering intensity for nanocavities formed on GMFs compared with the other two types due to the reduced loss (Figure 2h; Table S1, Supporting Information).

3.2. Simulations and Discussion

To further understand the observed difference in the optical response (Figure 2), we performed finite element method numerical simulations of near-field scattering of NSoM nanocavities formed on the studied gold mirrors (see Experimental Section). The effect of the difference in the dielectric functions (Figure 1j) of the SGFs, TSGFs, and GMFs on the optical response of NSoM nanocavities was first investigated (in this case, all of the gold films were assumed to have a smooth surface). Under transverse magnetic (TM) polarized light excitation (see Figure S8 in the Supporting Information for the excitation conditions and structural parameters used in the simulations), two resonance peaks (labeled as modes M and V, respectively) can be observed in the scattering spectra (Figure 3a) of the NSoM nanocavities formed on SGFs (green

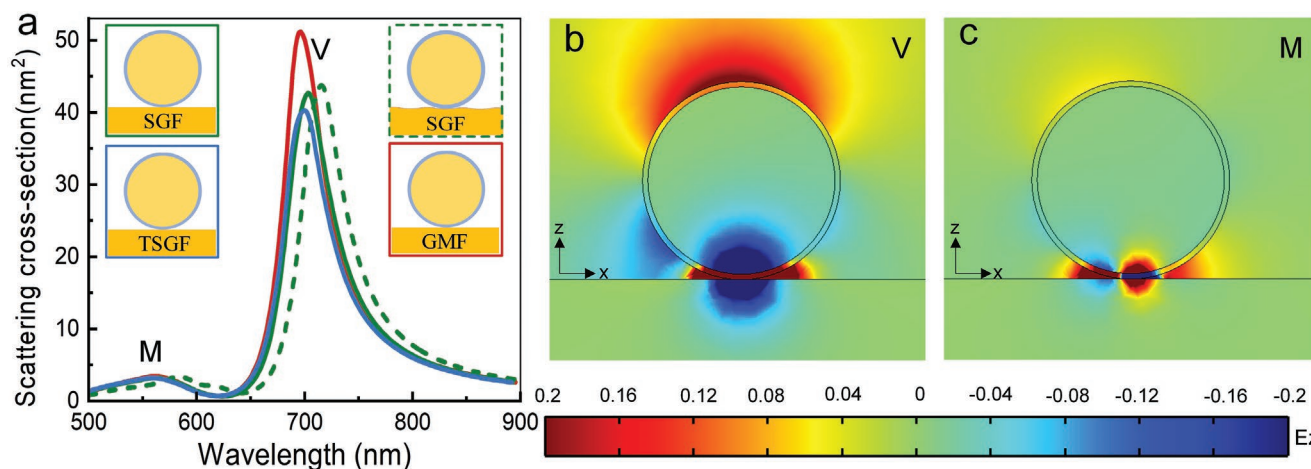


Figure 3. Numerical simulations of NSoM nanocavities formed on different gold films. a) Calculated scattering cross section of NSoM nanocavities formed on a smooth SGF (green line), a rough SGF (green dashed line), a smooth TSGF (blue line), a smooth GMF (red line). Inset: Schematics of NSoM nanocavities formed on different gold films. b,c) Normalized z -component electric near-field distributions of the two cavity modes labeled in panel (a) in the xz plane, perpendicular to the mirror and slicing through the center of the nanoparticle.

solid line), TSGFs (blue solid line), and GMFs (red solid line). They correspond to the excitation of the film-coupled vertical dipolar (Figure 3b) and quadrupolar (Figure 3c) modes of the nanosphere,^[46] respectively. It can be observed that the difference in the dielectric functions of the gold mirrors causes an obvious difference in the resonance peak wavelength of mode V (696.5, 700.0, and 701.9 nm for nanocavities formed on SGFs, TSGFs, and GMFs, respectively) and its intensity.

The effect of surface roughness on the optical response of the NSoM nanocavities formed on the SGFs with a rough surface is also important. According to the cross-sectional TEM image of an SGF shown in Figure 1h, instead of forming a point-contact gap, nanospheres investigated in the experiment, in fact, form a curved surface-contact gap with SGFs (as schematically shown in the inset of Figure 3a, outlined by dashed green line; see Figure S8b in the Supporting Information for the structural parameters used in the simulations). As a result, due to the increase in the contact area between the nanosphere and the mirror, compared with NSoM nanocavities formed on SGFs with a smooth surface, the simulated peak wavelength of mode V shows a redshift to 715.3 nm (Figure 3a, green dashed line). Therefore, the simulated peak wavelengths of mode V (located at 715.3, 700.0, and 701.9 nm for nanocavities formed on the SGFs with a rough surface, the TSGFs, and the GMFs, respectively) agree well with the experimentally measured results (average peak wavelengths of 712.2, 702.9, and 699.2 nm for nanocavities formed on SGFs, TSGFs, and GMFs, respectively). The mismatch between the scattering intensities for nanocavities formed on SGFs (dashed green line) and TSGFs (blue line) in the experimental and numerical results, can be related to underestimation of the role of the scattering of electrons on the rough surface in the simulation, which can be expected to be more pronounced in the case of highly localized modes, when surface effects play a bigger role. Particularly, this is important for rough SGFs, where the additional losses will lead to lower intensity and a smaller Q factor.

4. NCoM Nanocavities with a Face-Contact Gap

4.1. Experimental Results

In addition to the point-contact-type NSoM nanocavities investigated above, we further studied the effect of mirror quality on the optical response of face-contact-type NPoM nanocavities such as NCoM nanocavities. Experimentally, silver nanocubes with an average length of 77 ± 5 nm (Figure S3, Supporting Information) were used to construct the NCoM nanocavities on different gold films (with the same thickness of 50 nm). The total gap thickness is determined by the native polyvinyl pyrrolidone (PVP) layer on the surface of the nanocubes, which is measured to be ≈ 3.2 nm based on the TEM images (Figure S3, Supporting Information). Figure 4a–c presents typical dark-field scattering images of NCoM nanocavities formed on an SGF, a TSGF, and a GMF, respectively. Each nanocavity exhibits a scattering image consisting of a blue scattering spot at its center and a red ring-shaped scattering component around it. The same as in the case of NSoM nanocavities, the scattering images of NCoM nanocavities formed on the TSGF and GMF are more uniform than those formed on the SGF and the nanocavities formed on the GMF have the highest scattering intensity.

Figure 4d–f (see also Figure S6 in the Supporting Information) shows statistics of the dark-field scattering spectra of the nanocavities formed on the SGFs, TSGFs, and GMFs (≈ 100 nanocavities of each type were measured). Two resonance peaks located around 640 nm (labeled as mode V_1) and 730 nm (labeled as mode V_2) can be clearly observed in the scattering spectra. They stem from hybridization of the film-coupled vertical dipolar mode of the nanocube and one of the second-order Fabry–Perot modes of a metal–insulator–metal surface plasmon polariton supported by the nanocube–mirror gap.^[47,48] Similar to the NSoM nanocavities, the cavity-to-cavity homogeneity in the scattering spectra of the NCoM nanocavities formed on the TSGFs and GMFs is much better than that of

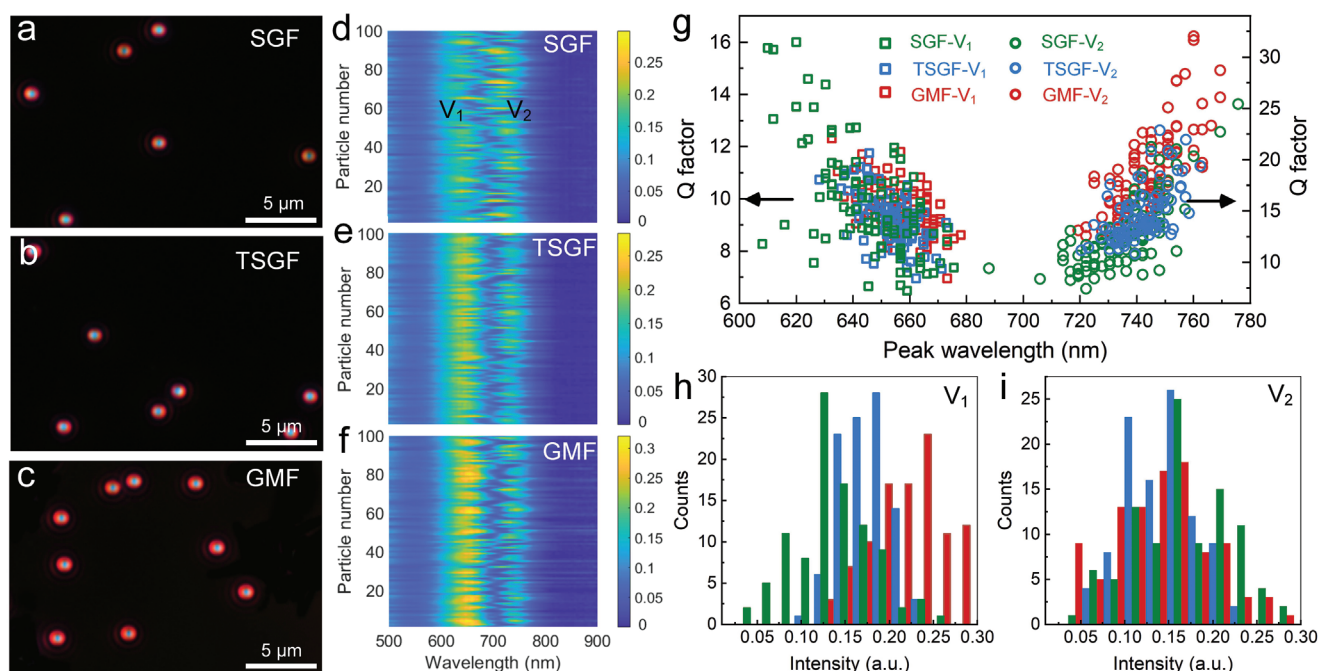


Figure 4. Statistical analysis of the effect of mirror quality on the optical response of NCoM nanocavities. a–c) Dark-field scattering images of NCoM nanocavities formed on a) an SGF, b) a TSGF, and c) a GMF. d–f) Waterfall plot of dark-field scattering spectra of the 100 nanocavities formed on the d) SGFs, e) TSGFs, and f) GMFs. g) Statistic plot of the peak wavelengths and quality factors of modes V_1 and V_2 (extracted from the scattering spectra shown in panels d)–f) for nanocavities formed on the SGFs (green), TSGFs (blue), and GMFs (red). h,i) Histogram of peak scattering intensities of modes h) V_1 and i) V_2 (extracted from the scattering spectra shown in panels d)–f) for nanocavities formed on the SGFs (green), TSGFs (blue), and GMFs (red).

the nanocavities formed on the SGFs. The two resonance modes of nanocavities formed on the TSGFs and GMFs also exhibit narrower linewidths corresponding to larger quality factors. This can be seen more explicitly in the statistic plot of the peak wavelengths and quality factors of the modes of each type of the nanocavities (Figure 4g; Table S2, Supporting Information). The average peak wavelengths for modes V_1 and V_2 are 645.5 ± 15.5 , 653.8 ± 8.9 , and 657.6 ± 9.1 nm and 735.1 ± 13.5 , 741.7 ± 8.5 , and 744.1 ± 9.8 nm for nanocavities formed on the SGFs, TSGFs, and GMFs, respectively. The NCoM nanocavities formed on the TSGFs and GMFs have a better homogeneity in the scattering spectrum, which is again due to the great improvement in their surface quality compared with the SGFs, leading to the minimization of fluctuations in the gap morphology (the interface profile and gap thickness). Different to the case of the NSoM nanocavities, NCoM nanocavities formed on SGFs demonstrate a blueshift (≈ 10 nm) in the average peak wavelength of the two modes compared with NCoM nanocavities formed on the TSGFs and GMFs. This is caused by the increase of an equivalent gap thickness for face-contact-type NCoM nanocavities formed on rough (i.e., SGFs) gold mirrors, which will be discussed in detail later.

Due to the improvement in surface roughness and crystal-line quality from SGFs to TSGFs and GMFs, the quality factors of modes V_1 and V_2 (at the same resonance wavelengths) of NCoM nanocavities increase (Figure 4g). It is worth noting that, for each type of the NCoM nanocavities, the statistic distributions of the quality factors decrease gradually with the increase of peak wavelength for mode V_1 , while increase gradually with

the increase of peak wavelength for mode V_2 , showing an overall “V-shaped” distribution. This can be attributed to the change in the interaction between the film-coupled vertical dipolar mode of the nanocube and the second-order Fabry–Perot mode of a metal–insulator–metal surface plasmon polariton supported by the nanocube–mirror gap (the coupling between them resulting in the generation of modes V_1 and V_2) due to a fluctuation in the size of the nanocubes. The closer the resonance wavelength of modes V_1 or V_2 to the resonance wavelength of the film-coupled vertical dipolar mode of the nanocube with high radiation efficiency, the higher the radiation of the mode to the far field, which results in a lower quality factor. Figure 4h,i shows the distribution of extracted peak intensities of modes V_1 and V_2 . Generally, nanocavities based on GMFs have a potential for stronger scattering intensity due to the reduction in the loss of the mirror (Figure 4h; Table S2, Supporting Information). However, due to the lower radiation efficiency of mode V_2 for NCoM nanocavities formed on GMFs, they have similar scattering intensities with that of mode V_2 for NCoM nanocavities formed on SGFs and TSGFs (Figure 4i).

4.2. Simulations and Discussion

We also performed simulations of near-field scattering of NCoM nanocavities formed on different types of gold mirrors (see Experimental Section). The effect of the difference in the dielectric functions (Figure 1j) of the SGFs, TSGFs, and GMFs on the optical response was first investigated. Under TM

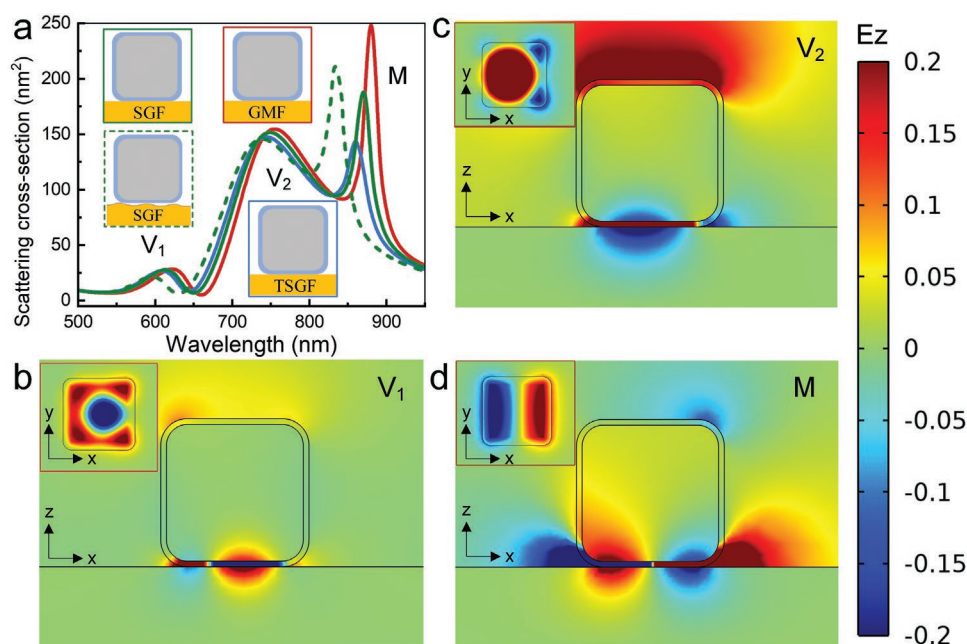


Figure 5. Numerical simulations of NCoM nanocavities formed on different gold films. a) Calculated near-field scattering cross section of NCoM nanocavities formed on a smooth SGF (green line), a rough SGF (green dashed line), a smooth TSGF (blue line), and a smooth GMF (red line). Insets: Schematics of NCoM nanocavities formed on different gold films. b–d) Normalized z -component electric near-field distributions of the cavity modes labeled in panel (a) in the xz plane, perpendicular to the mirror and slicing through the center of the nanocube. Inset: The near-field distributions in the plane slicing through the middle of the gap.

excitation (see Figure S8 in the Supporting Information for the excitation conditions and structural parameters used in the simulations), three resonance peaks (labeled as modes V_1 , V_2 , and M) can be observed in the scattering spectra (Figure 5a) of NCoM nanocavities formed on the SGFs (green solid line), TSGFs (blue solid line), and GMFs (red solid line). Scattered near-field distributions of modes V_1 , V_2 , and M shown in Figure 5b–d confirm the nature of these modes, in which the coupling between the film-coupled vertical dipolar mode of the nanocube and a second-order Fabry–Perot mode of a metal–insulator–metal surface plasmon polariton supported by the nanocube–mirror gap can be clearly seen for modes V_1 and V_2 (Figure 5b,c), and the coupling between the transversal dipolar mode of the nanocube and the mirror can be seen for mode M (Figure 5d). The absence of mode M in the measured scattering spectra (Figure 4d–f) is due to a limited measurement capability of the setup at wavelengths larger than 850 nm. Similarly, the difference in the dielectric functions of the gold mirrors causes an obvious variation in the resonance wavelength and intensity of the modes.

The simulated resonance wavelengths of modes V_1 and V_2 for nanocavities formed on the TSGFs and GMFs agree well with the experimentally measured results. However, for nanocavities formed on SGFs, compared with the simulated resonance wavelengths of modes V_1 and V_2 , the measured results blueshift by about 10 nm. When the surface roughness of the SGF was taken into consideration in the simulation (dashed green line squared schematic in the inset of Figure 5a; see Figure S8b in the Supporting Information for the structural parameters used in the simulations), the resonance wavelengths of modes V_1 and V_2 show an ≈ 10 nm blueshift (Figure 5a, dashed green

line), therefore, agreeing well with the experimental results. The blueshift of the resonance wavelength of the modes of the NCoM nanocavities is due to the increase of the equivalent gap thickness for nanocavities with face-contact gaps.

5. Conclusion

We have demonstrated both experimentally and theoretically that the mirror quality has a significant influence on the optical response of NPoM nanocavities. Surface roughness of the metal mirrors can introduce a significant change in the gap morphology, resulting in a deterioration of the cavity-to-cavity homogeneity of the optical response, as well as a shift in the peak wavelengths of resonance modes in comparison with nanocavities formed on smooth mirrors. In this study, films with a thickness of 50 nm were used: for thinner films, we may expect the observed effects to be even more important. Overall, single-crystalline GMFs provide an attractive platform for the construction of high-quality NPoM nanocavities in terms of higher cavity-to-cavity homogeneity in the optical response and lower optical loss, especially when the mirror thickness is further decreased, compared with deteriorated film quality for SGFs and TSGFs.^[39] These are required, for example, for the precise match of the resonance modes of nanocavities with quantum emitters and, therefore, the enhancement of spontaneous emission.^[49] However, for the construction of large-scale nanocavity arrays, TSGFs with excellent surface smoothness are recommended due to the limited lateral size (around several hundred micrometers) of the GMFs. These observations improve the understanding of optical properties of the

nanocavity and provide guidelines for the design of nanocavity-based devices with optimized performance for practical applications.

6. Experimental Section

Preparation of Gold Mirrors: To avoid the use of metallic adhesion layers (such as Cr and Ti) that can introduce significant optical loss to plasmonic structures,^[50] cleaned glass slides (10127101P-G, CITOGlas) were first functionalized with a monolayer of (3-aminopropyl) trimethoxysilane instead for the subsequent deposition of gold. This was realized by immersing them into a 5 mm (3-aminopropyl) trimethoxysilane (97%, Sigma-Aldrich) ethanol solution overnight and kept at 80 °C for 1 h to enhance the attachment of (3-aminopropyl) trimethoxysilane molecules on the glass slide surface. The functionalized glass slides were rinsed with excessive ethanol and dried with nitrogen. SGFs were prepared by depositing gold onto as-prepared glass substrates by magnetron sputtering (DISCOVERY-635) at a base pressure of $\approx 5 \times 10^{-6}$ Torr and a deposition rate of 10 Å s^{-1} . TSGFs were obtained as follows. First, gold films with a thickness of 50 nm were deposited onto cleaned silicon substrates by magnetron sputtering as described above. Second, a droplet (10 μL) of epoxy glue (EPO-TEK 301-2) was admitted onto the gold films, followed by the placement of cleaned glass substrates on the top. Third, the structures were transferred onto a hot plate to cure the epoxy under 80 °C for 3 h, and then slowly cooled down to room temperature. Finally, the glass substrates were detached from the silicon substrates with gold films having an atomically smooth surface attached to them.

GMFs were synthesized using a wet chemical approach.^[39] First, a growth solution was prepared by the addition of an aqueous HAuCl_4 (0.025 M, 360 μL) into a 10 mL of ethylene glycol in a 20 mL glass vial. Then, a cleaned glass (10127101P-G, CITOGlas) was immersed into the solution at a slightly tilted angle. Finally, the growth solution was stored in an oven at a constant temperature of 95 °C for about 7 h for the growth of GMFs on the substrate. After the growth, the glass substrate with GMFs on the surface was cleaned with ethanol, dried in a nitrogen environment for further use. As-fabricated GMFs were treated with oxygen plasma cleaning to remove the native organic layer before the fabrication of the NPoM nanocavities.

Measurement of Dielectric Functions: An imaging ellipsometer (NanoFilm EP4) was used to measure the dielectric functions of the three types of gold mirrors (Figure S2, Supporting Information). The samples were measured in the wavelength range from 400 to 980 nm under an incidence angle of 50°, with the analyzed area fixed at $\approx 80 \times 80 \mu\text{m}^2$. The four-zone measurement method was applied to minimize measurement errors.^[51] Then, the amplitude ratio (Ψ) and phase difference (Δ) were determined from the rotational angles of the polarizer and analyzer when the detected light intensity was zero. Finally, the dielectric functions of the gold films were derived from the measured Ψ and Δ by assuming a three-layer model (air, gold, and glass substrate) and applying the Fresnel equations. The thickness of the glass substrate could be considered to be infinite, and the thickness of gold films was 200 nm. The spectra of Ψ and Δ were fitted by the appendant data processing software of the ellipsometer to obtain the values of n and k . A superimposed line shape (Drude + Three-Lorentz) was used to fit the experimentally measured data. During the fitting procedure, the root-mean-square error was minimized. Finally, from the obtained n and k , it was calculated the complex permittivity $\epsilon = \epsilon_1 + i\epsilon_2$. Fitting parameters can be found in Table S3 (Supporting Information).

Numerical Simulations: The electromagnetic response of nanocavities was numerically simulated using a finite-element method (COMSOL Multiphysics software). The scattering from a single nanocavity was computed using a scattered-field formulation, in which the scattered fields were presented as an addition to the analytical solution for an incident plane wave caused by the presence of the nanostructure. Gold nanospheres and silver nanocubes were both modeled as core-shell

structures (see Figure S8 in the Supporting Information for the excitation conditions and structural parameters used in the simulations) in agreement with the experiment. Particularly, the nanocube corners were rounded with a 15 nm radius to match the experimental samples. The entire NPoM structure was illuminated with a p-polarized plane wave at 68° (the same as the incident angle of the illumination light in the experiments). The wavelength of the incident wave was varied from 500 to 950 nm, and the scattered light was then collected within a cone having a half-angle of $\theta = 25^\circ$ corresponding to the numerical aperture (NA) of the objective used in the experiments. The partial near-field scattering cross section was obtained by dividing the obtained power flow integral by the intensity of the incident wave. The glass substrate was assumed to be semi-infinite and had a refractive index of 1.45. The refractive index of the CTAC and PVP surfactant polymer was taken to be 1.4 and 1.55, respectively.^[52,53]

Supporting Information

Supporting Information is available from the Wiley Online Library or from the author.

Acknowledgements

The authors thank Yuanbiao Tong and Jiajie Zhu for helpful discussions. This research was supported by the National Natural Science Foundation of China (Grant Nos. 62075195, 1200433, 92150302, 12174202, and 92050114), and Fundamental Research Funds for the Central Universities (Grant No. 226-2022-00147). A.V.K. and A.V.Z. were supported by EPSRC (UK) (Grant No. EP/W017075/1), and the ERC iCOMM Project (Project No. 789340).

Conflict of Interest

The authors declare no conflict of interest.

Data Availability Statement

The data that support the findings of this study are available from the corresponding author upon reasonable request.

Keywords

dielectric function, mirror quality, nanocavities, nanoparticle on mirror, plasmons

Received: August 16, 2022

Revised: November 6, 2022

Published online: December 4, 2022

- [1] D. K. Gramotnev, S. I. Bozhevolnyi, *Nat. Photonics* **2010**, 4, 83.
- [2] J. A. Schuller, E. S. Barnard, W. Cai, Y. C. Jun, J. S. White, M. L. Brongersma, *Nat. Mater.* **2010**, 9, 193.
- [3] C. Ciraci, R. T. Hill, J. J. Mock, Y. Urzhumov, A. I. Fernández-Domínguez, S. A. Maier, J. B. Pendry, A. Chilkoti, D. R. Smith, *Science* **2012**, 337, 1072.
- [4] P. Wang, A. V. Krasavin, L. Liu, Y. Jiang, Z. Li, X. Guo, L. Tong, A. V. Zayats, *Chem. Rev.* **2022**, 122, 15031.
- [5] S. Nie, S. R. Emory, *Science* **1997**, 275, 1102.

- [6] H. Xu, E. J. Bjerneld, M. Käll, L. Börjesson, *Phys. Rev. Lett.* **1999**, *83*, 4357.
- [7] S. Kühn, U. Håkanson, L. Rogobete, V. Sandoghdar, *Phys. Rev. Lett.* **2006**, *97*, 017402.
- [8] R. F. Oulton, V. J. Sorger, T. Zentgraf, R.-M. Ma, C. Gladden, L. Dai, G. Bartal, X. Zhang, *Nature* **2009**, *461*, 629.
- [9] M. Kauranen, A. Zayats, *Nat. Photonics* **2012**, *6*, 737.
- [10] W. Zhou, M. Dridi, J. Y. Suh, C. H. Kim, D. T. Co, M. R. Wasielewski, G. C. Schatz, T. W. Odom, *Nat. Nanotechnol.* **2013**, *8*, 506.
- [11] Y. Liang, C. Li, Y.-Z. Huang, Q. Zhang, *ACS Nano* **2020**, *14*, 14375.
- [12] P. Wang, M. E. Nasir, A. V. Krasavin, W. Dickson, Y. Jiang, A. V. Zayats, *Acc. Chem. Res.* **2019**, *52*, 3018.
- [13] J. Li, A. V. Krasavin, L. Webster, P. Segovia, A. V. Zayats, D. Richards, *Sci. Rep.* **2016**, *6*, 21349.
- [14] G.-C. Li, Q. Zhang, S. A. Maier, D. Lei, *Nanophotonics* **2018**, *7*, 1865.
- [15] J. J. Baumberg, J. Aizpurua, M. H. Mikkelsen, D. R. Smith, *Nat. Mater.* **2019**, *18*, 668.
- [16] K. J. Russell, T.-L. Liu, S. Cui, E. L. Hu, *Nat. Photonics* **2012**, *6*, 459.
- [17] G. M. Akselrod, C. Argyropoulos, T. B. Hoang, C. Ciraci, C. Fang, J. Huang, D. R. Smith, M. H. Mikkelsen, *Nat. Photonics* **2014**, *8*, 835.
- [18] T. B. Hoang, G. M. Akselrod, C. Argyropoulos, J. Huang, D. R. Smith, M. H. Mikkelsen, *Nat. Commun.* **2015**, *6*, 7788.
- [19] T. W. Lo, X. Chen, Z. Zhang, Q. Zhang, C. W. Leung, A. V. Zayats, D. Lei, *Nano Lett.* **2022**, *22*, 1915.
- [20] G.-C. Li, D. Lei, M. Qiu, W. Jin, S. Lan, A. V. Zayats, *Nat. Commun.* **2021**, *12*, 4326.
- [21] A. W. Powell, D. M. Coles, R. A. Taylor, A. A. R. Watt, H. E. Assender, J. M. Smith, *Adv. Opt. Mater.* **2016**, *4*, 634.
- [22] W. Chen, S. Zhang, Q. Deng, H. Xu, *Nat. Commun.* **2018**, *9*, 801.
- [23] R. Chikkaraddy, B. de Nijs, F. Benz, S. J. Barrow, O. A. Scherman, E. Rosta, A. Demetriadou, P. Fox, O. Hess, J. J. Baumberg, *Nature* **2016**, *535*, 127.
- [24] M.-E. Kleemann, R. Chikkaraddy, E. M. Alexeev, D. Kos, C. Carnegie, W. Deacon, A. C. de Pury, C. Große, B. de Nijs, J. Mertens, A. I. Tartakovskii, J. J. Baumberg, *Nat. Commun.* **2017**, *8*, 1296.
- [25] G. Hajisalem, M. S. Nezami, R. Gordon, *Nano Lett.* **2014**, *14*, 6651.
- [26] M. Parzefall, Á. Szabó, T. Taniguchi, K. Watanabe, M. Luisier, L. Novotny, *Nat. Commun.* **2019**, *10*, 292.
- [27] P. Wang, A. V. Krasavin, M. E. Nasir, W. Dickson, A. V. Zayats, *Nat. Nanotechnol.* **2018**, *13*, 159.
- [28] J. J. Mock, R. T. Hill, A. Degiron, S. Zauscher, A. Chilkoti, D. R. Smith, *Nano Lett.* **2008**, *8*, 2245.
- [29] H. Chen, T. Ming, S. Zhang, Z. Jin, B. Yang, J. Wang, *ACS Nano* **2011**, *5*, 4865.
- [30] F. Benz, R. Chikkaraddy, A. Salmon, H. Ohadi, B. de Nijs, J. Mertens, C. Carnegie, R. W. Bowman, J. J. Baumberg, *J. Phys. Chem.* **2016**, *7*, 2264.
- [31] M.-E. Kleemann, J. Mertens, X. Zheng, S. Cormier, V. Turek, F. Benz, R. Chikkaraddy, W. Deacon, A. Lombardi, V. V. Moshchalkov, G. A. E. Vandenbosch, J. J. Baumberg, *ACS Nano* **2017**, *11*, 850.
- [32] S. Mubeen, S. Zhang, N. Kim, S. Lee, S. Krämer, H. Xu, M. Moskovits, *Nano Lett.* **2012**, *12*, 2088.
- [33] A. Moreau, C. Ciraci, J. J. Mock, R. T. Hill, Q. Wang, B. J. Wiley, A. Chilkoti, D. R. Smith, *Nature* **2012**, *492*, 86.
- [34] D. Y. Lei, A. I. Fernández-Domínguez, Y. Sonnefraud, K. Appavoo, R. F. Haglund, J. B. Pendry, S. A. Maier, *ACS Nano* **2012**, *6*, 1380.
- [35] A. V. Krasavin, *J. Phys. Photonics* **2021**, *3*, 042006.
- [36] N. Vogel, J. Zieleniecki, I. Köper, *Nanoscale* **2012**, *4*, 3820.
- [37] J. Peng, H.-H. Jeong, Q. Lin, S. Cormier, H.-L. Liang, M. F. L. D. Volder, S. Vignolini, J. J. Baumberg, *Sci. Adv.* **2019**, *5*, eaaw2205.
- [38] C. Schörner, M. Lippitz, *J. Chem. Phys.* **2021**, *155*, 234202.
- [39] L. Liu, A. V. Krasavin, J. Zheng, Y. Tong, P. Wang, X. Wu, B. Hecht, C. Pan, J. Li, L. Li, X. Guo, A. V. Zayats, L. Tong, *Nano Lett.* **2022**, *22*, 1786.
- [40] C. Lumdee, B. Yun, P. G. Kik, *Nanoscale* **2015**, *7*, 4250.
- [41] F. Kiani, G. Tagliabue, *Chem. Mater.* **2022**, *34*, 1278.
- [42] P. B. Johnson, R. W. Christy, *Phys. Rev. B* **1972**, *6*, 4370.
- [43] R. L. Olmon, B. Slovick, T. W. Johnson, D. Shelton, S.-H. Oh, G. D. Boreman, M. B. Raschke, *Phys. Rev. B* **2012**, *86*, 235147.
- [44] D. E. Aspnes, E. Kinsbron, D. D. Bacon, *Phys. Rev. B* **1980**, *21*, 3290.
- [45] Y. Zheng, X. Zhong, Z. Li, Y. Xia, *Part. Part. Syst. Character.* **2014**, *31*, 266.
- [46] G.-C. Li, Y.-L. Zhang, D. Y. Lei, *Nanoscale* **2016**, *8*, 7119.
- [47] R. Chikkaraddy, X. Zheng, F. Benz, L. J. Brooks, B. de Nijs, C. Carnegie, M.-E. Kleemann, J. Mertens, R. W. Bowman, G. A. E. Vandenbosch, V. V. Moshchalkov, J. J. Baumberg, *ACS Photonics* **2017**, *4*, 469.
- [48] J. B. Lassiter, F. McGuire, J. J. Mock, C. Ciraci, R. T. Hill, B. J. Wiley, A. Chilkoti, D. R. Smith, *Nano Lett.* **2013**, *13*, 5866.
- [49] T. B. Hoang, G. M. Akselrod, M. H. Mikkelsen, *Nano Lett.* **2016**, *16*, 270.
- [50] T. G. Habteyes, S. Dhuey, E. Wood, D. Gargas, S. Cabrini, P. J. Schuck, A. P. Alivisatos, S. R. Leone, *ACS Nano* **2012**, *6*, 5702.
- [51] A. Matković, A. Beltaos, M. Milićević, U. Ralević, B. Vasić, D. Jovanović, R. Gajić, *J. Appl. Phys.* **2012**, *112*, 123523.
- [52] T. A. F. König, P. A. Ledin, J. Kerszulis, M. A. Mahmoud, M. A. El-Sayed, J. R. Reynolds, V. V. Tsukruk, *ACS Nano* **2014**, *8*, 6182.
- [53] N. Slesiona, S. Thamm, H. L. K. S. Stolle, V. Weisenborn, P. Müller, A. Csáki, W. Fritzsche, *Nanomaterials* **2020**, *10*, 1119.